

Wind Tunnel Tests on Flow Characteristics of the KRISO 3,600 TEU Containership and 300K VLCC Double-Deck Ship Models

Sang-Joon Lee,* Hak-Rok Kim,* Wu-Joan Kim,† and Suak-Ho Van†

* Department of Mechanical Engineering, Pohang University of Science and Technology, Pohang, Korea

† Ship Performance Department, Korea Research Institute of Ships and Ocean Engineering, Yosung-Ku, Taejon, Korea

The flow characteristics in the stern and near-wake region of two ship models, the Korea Research Institute of Ships and Ocean Engineering (KRISO) 3,600 TEU containership (KCS) and the KRISO 300K very large crude oil carrier (VLCC) (KVLCC), were investigated experimentally. The double-deck ship models were installed in a subsonic wind tunnel. The freestream velocity was fixed at $U_0 = 25$ m/s, and the corresponding Reynolds numbers based on the model length (L_{pp}) were about 3.3×10^6 and 4.6×10^6 for the KCS and KVLCC models, respectively. The spatial distributions of mean velocity components and turbulence statistics, including turbulence intensities, Reynolds shear stresses, and turbulent kinetic energy, were measured using a hot-wire anemometer. For both ship models, the stern flow and near-wake show very complicated three-dimensional flow patterns. The longitudinal vortices formed in the stern region dominantly influence the flow structure in the near-wake region. In the region of main longitudinal vortices, the mean velocity deficits and all turbulence statistics have large values, compared with the surrounding flow. As the flow moves downstream, the turbulence statistics increase and have maximum values at the after-perpendicular (AP) plane and then decrease gradually due to the expansion of the shear layer. For the KVLCC model, the spatial distributions of mean velocity components and turbulence intensities behind the propeller plane clearly show hook-shaped contours. These experimental results, especially the turbulence statistics, can be used not only to understand the flows around modern practical hull forms but also to validate the computational fluid dynamics codes and turbulence models. The complete experimental data set is available on the website (<http://www.postech.ac.kr/me/efml/data>).

Introduction

The operational cost of a ship can be reduced by improving the ship performance. Flow information on the stern and near-wake region has been used for determining ship resistance and for the design of propellers and appendages. However, the flow structure around a ship is very complex and varies largely in the stern and wake region depending on the ship hull form. Therefore, accurate measurement or precise numerical predictions of flow around a ship, especially the turbulence statistics of the stern and wake flow, are very important for practical ship design.

Several numerical and experimental studies have been carried out to investigate flow around relatively simple and idealized hull forms. Larsson (1974) and Hoffman (1976) measured the mean flow structure of turbulence boundary layers developed on ship hulls. Löfdahl (1982) measured the mean velocities and Reynolds stresses in the stern region of a Service and Support Professionals Association (SSPA) 720 liner. Knaack et al (1985) measured some turbulence data for a Hamburg Ship Model Basin (HSVA) tanker in the stern and near-wake region. For a Wigley hull form, Patel and Sarda (1990) carried out a wind tunnel test using a double-deck model, in which they measured pressure, mean velocities, and Reynolds stresses in the region from midship to almost a ship length downstream. However, the hull forms used in these previous studies are somewhat simple and idealized (ITTC 1987,

Manuscript received at SNAME headquarters August 5, 1999; revised manuscript received April 26, 2002.

Toda et al 1988). Therefore, the flow structures are more or less different from those of modern hull forms.

In order to predict the details of ship stern and wake flows, many numerical studies have been performed and several workshops were organized to assess the relative merits of different approaches and to identify critical research areas in need of further study. For example, the Gothenburg 2000 Workshop on computational fluid dynamics (CFD) in ship hydrodynamics dealt with three different ship models (Larsson et al 2000); one was the David Taylor Model Basin (DTMB) model 5415 and the others were the Korea Research Institute of Ships and Ocean Engineering (KRISO) 3,600 TEU containership (hereafter, KCS) and the KRISO 300K very large crude oil carrier (VLCC) (hereafter, KVLCC) of the present paper. Nowadays, with the rapid advances of computers, numerical simulations can predict the details of the flow around a ship hull form. However, these numerical studies on flow around a ship model have some difficulties due to lack of comparable experimental data, especially turbulence statistics in the stern and wake regions. For developing reliable numerical methods and better understanding of the flow around a real ship, it is necessary to accumulate experimental benchmark data on practical hull forms of modern ships.

Most previous experimental studies on ship hydrodynamics have been carried out using a towing tank. Hockstra and Aallers (1997) measured the macro wake of various hull forms (including tankers, containerships, and frigates) and investigated the wake structures and the rudder effects in detail. Recently, Kim et al (2001) measured flows around modern commercial ship models. However, it is difficult to get spatial distribution of turbulence statistics from the towing tank experiments.

In this study, the flow characteristics in the stern and near-wake region of the KCS and KVLCC hull forms were investigated experimentally. The main objectives of this study are to accumulate reliable experimental data for each ship model to validate CFD tools in ship hydrodynamics and to understand the flows around modern commercial hull forms in more detail. The spatial distributions of mean velocity components, Reynolds stresses, and turbulent kinetic energy at several transverse stations were measured and discussed in this study. At the recent Gothenburg 2000 workshop, present data for KVLCC were used as a test case for turbulence modeling. Because the KCS hull form was used as a test case for propeller–hull interaction, however, the present wind tunnel data were not used at the workshop. Therefore, the turbulence statistics for the KCS model can be used for additional CFD validation efforts and physical understanding.

Experimental apparatus and procedure

Wind tunnel and ship model

Experiments were carried out in a closed-type Pohang University of Science and Technology subsonic wind tunnel having a test section of $1.8^W(\text{m}) \times 1.5^H(\text{m}) \times 4.3^L(\text{m})$. The maximum wind speed is 70 m/s, and the free-stream turbulence intensity is less than 0.15%. Air temperature in the wind tunnel test section was maintained at an accuracy of $\pm 0.1^\circ\text{C}$ using an internal heat exchanger.

The double-deck-shaped KCS model has a length (L_{pp}) between perpendiculars of 2 m, breadth (B) of 0.28 m, draft (D) of 0.2 m, and block coefficient (C_B) of 0.65. On the other hand,

Table 1 Principal dimensions of two models (unit; m)

| | KCS Ship | | KVLCC Ship | |
|--------------------------|--------------------|------------|--------------------|------------|
| | Full-scale Ship | Model Ship | Full-scale Ship | Model Ship |
| Length, L_{pp} | 230.0 | 2.0 | 320 | 2.7586 |
| Breadth, B | 32.2 | 0.28 | 58.0 | 0.5 |
| Depth, D | 23.0 | 0.2 | 30.0 | 0.2586 |
| Draft, T | 10.8 | 0.0939 | 20.8 | 0.1793 |
| Block coefficient, C_B | | 0.65 | | 0.8098 |
| Scale ratio, χ | | 115 | | 116 |

KCS = Korea Research Institute of Ships and Ocean Engineering (KRISO) 3,600 TEU containership; KVLCC = KRISO 300K VLCC.

the KVLCC model has a length (L_{pp}) of 2.7586 m, breadth (B) of 0.5 m, draft (D) of 0.1793 m, and block coefficient (C_B) of 0.8098. They were made of seasoned wood, and their scale ratios for the prototype KCS and KVLCC ships are 1/115 and 1/116, respectively. The principal dimensions of the two experimental models are listed in Table 1. Figure 1 shows the body plans of two ship models tested in this study. When the double-deck ship model was installed in the wind tunnel, the blockage ratios in the test section were about 6.6% and 1.9% for the KVLCC and KCS models. Therefore, no velocity correction for blockage effect was made.

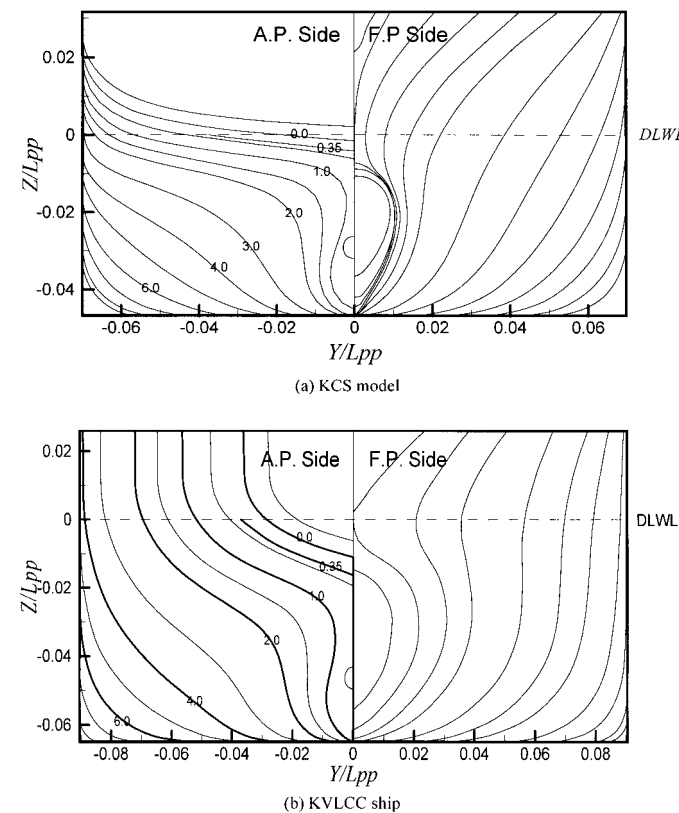


Fig. 1 Body plan of ship models used in this study. A.P. = after perpendicular; DLWL = design load water line; F.P. = fore perpendicular; KCS = Korea Research Institute of Ships and Ocean Engineering (KRISO) 3,600 TEU containership; KVLCC = KRISO 300K VLCC

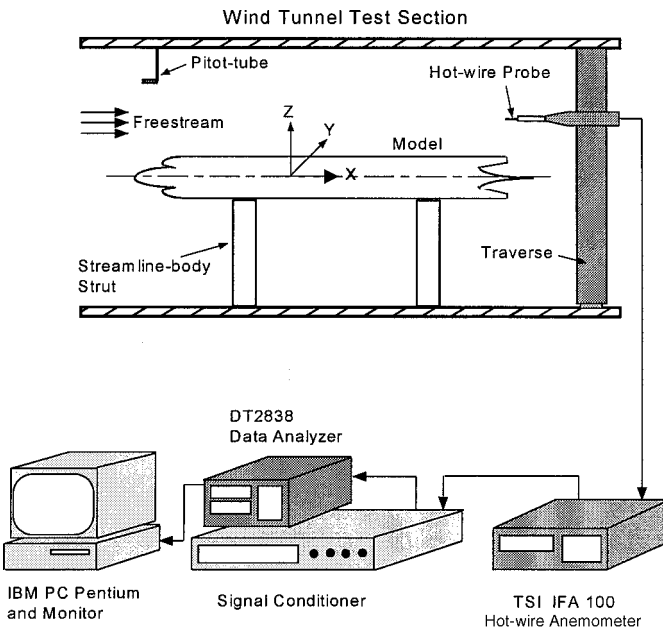


Fig. 2 Schematic diagram of experimental apparatus and coordinate system

During experiments, the free-stream velocity was fixed at $U_0 = 25$ m/s and the corresponding Reynolds numbers based on the model length (L_{pp}) were 3.3×10^6 and 4.6×10^6 for KCS and KVLCC models. In order to stimulate turbulent flow, two rows of cylindrical studs, 2 mm high and 1.4 mm in diameter, were installed at Station 19 and Station 20.3 of the KCS model with studs placed at intervals of 10 mm. For the KVLCC model, two rows of cylindrical studs, 2 mm high and 1.6 mm in diameter, were installed at Station 19 and Station 20.25 with studs placed at intervals of 10 mm. Each ship model was fixed to the bottom of the wind tunnel test section with two streamlined struts, as shown in Fig. 2, to reduce flow-induced structural vibration.

Measurement procedure

Figure 2 shows the schematic diagram of the experimental apparatus and coordinate system used in this study. The positive directions of Cartesian coordinates X, Y, Z are defined as downstream direction from bow to stern, from the centerplane toward the starboard side, and from the waterplane toward the keel, respectively. Flow velocity around the ship model was measured with a hot-wire x -probe (Dantec 55P61). The analog output signals from the hot-wire anemometer (TSI IFA-100) were low-pass filtered at 800 Hz and digitized by an A/D converter (DT2838) at the sampling rate of 4,000 samples per second. They were statistically averaged to obtain the mean velocities and turbulence statistics.

The hot-wire probe was traversed precisely using a computer-controlled traverse device. The probe was moved in the Cartesian coordinate system, not in the boundary layer coordinate. The maximum error over the entire traverse movements was within the acceptable limit of about 0.5 mm. The hot-wire probe was calibrated before and after each experiment. From the effective yaw angle calibration, the yaw angles ψ_1, ψ_2 were found to be 44.62 and 43.61 degrees, respectively. The velocity measurements were performed in the upper symmetric side ($Z > 0$) of

the double-deck model to reduce flow disturbance caused by the supporting struts located in the lower side.

In this experiment, an oil film method was employed to visualize limiting streamlines on the hull surface. The hull surface was coated uniformly with the oil mixed with $PbCrO_4$ powder. As the wind tunnel starts, the oil film on the surface moves to the direction of local shear forces. A Nikon F5 camera was used to capture the oil patterns reflecting the spatial distribution of wall shear stress.

Experimental uncertainties

Uncertainty analysis was carried out for the measured data following the procedure recommended by the International Towing Tank Conference (ITTC 1999) to ascertain the error bounds of measurement results. This gives 95% confidence estimates of the precision limits.

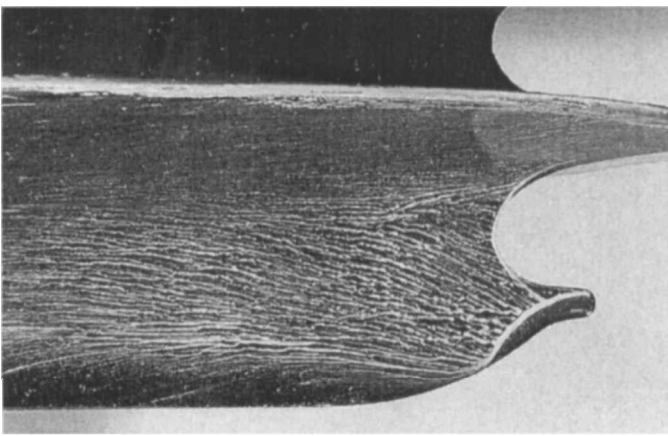
The error analysis was conducted mainly on the vertical (centerplane, $Y = 0$) and horizontal (waterplane, $Z = 0$) planes of symmetry of the stern and near-wake region. The mean velocities and Reynolds stresses revealed that the flow is well symmetry with respect to the symmetry planes of the ship model. The estimated uncertainty for the magnitude of the axial mean velocity component was about 0.5%, and that of the transverse flow (V, W) was less than 1.0%. The directional angle of the mean streamwise velocity has an error of about 1.5 degrees. The Reynolds stresses \bar{u}^2 and $\bar{u}'v'$ have uncertainties of about 7.8% and 8.5%, respectively. The maximum error for the turbulent kinetic energy was about 12.8%. The estimated uncertainties for all measured physical quantities are summarized in Table 2.

The higher-order turbulence statistics have a larger error than that of the mean velocity components. These errors are attributed to the factors of finite size and wall proximity effect of the hot-wire sensor, interference of strut and model, mismatch of reference direction, and so forth (Patel 1988).

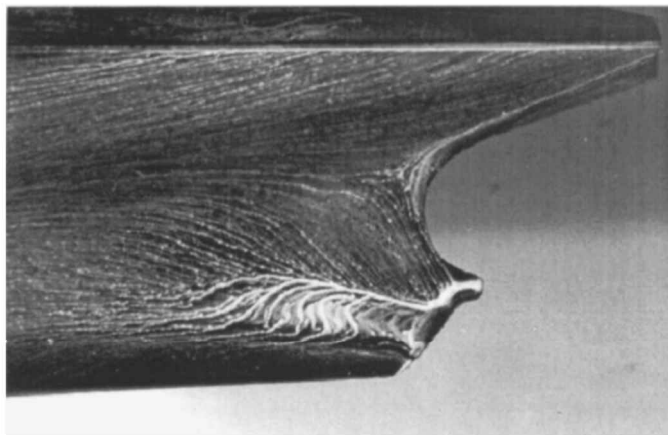
The hull forms and the complete experimental data set tested in this research are available on the website (<http://www.postech.ac.kr/me/efml/data>).

Table 2 Experimental uncertainties of measured quantities
(unit: %)

| Quantity | Uncertainty |
|----------------------------|-------------------|
| Magnitude of mean velocity | $ U $ 0.5 |
| | $ V $ 0.7 |
| | $ W $ 1.0 |
| Angle of mean velocity | Angle of U 0.5° |
| | Angle of V 0.5° |
| | Angle of W 0.7° |
| Reynolds normal stress | \bar{u}^2 7.8 |
| | \bar{v}^2 12.1 |
| | \bar{w}^2 14.7 |
| Reynolds shear stress | $\bar{u}'v'$ 8.5 |
| | $\bar{u}'w'$ 17.5 |
| Turbulent kinetic energy | k 12.8 |



(a) KCS double model



(b) KVLCC double model

Fig. 3 Visualized limiting streamlines on the hull surface in the stern region. KCS = Korea Research Institute of Ships and Ocean Engineering (KRISO) 3,600 TEU containership; KVLCC = KRISO 300K VLCC

Results and discussion

Limiting streamlines

Figure 3 shows typical visualized flow on the hull surface in the stern region for two ship models. The oil pattern on the hull surface exhibits complicated limiting streamlines caused by wall shear stresses (Gietz & Kux 1995). It clearly shows the lines of flow convergence merged at the propeller boss. The flow can be subdivided into three parts. One is the upper half region in which flow moves upward to the waterline. In the middle region, the flow moves downward diagonally to the propeller boss. In the region near the keel, the flow moves upward diagonally with lines of flow convergence and forms an asymptotic line. Then it approaches the propeller boss at the stern end. Comparing two ship models, the limiting streamlines of the KVLCC model deflect largely in the region between the keel and the propeller boss. This indicates that the longitudinal vortices formed around the stern of the KVLCC model are much stronger and elongated vertically, compared with the KCS model. This may be attributed

to the formation of a large-scale secondary vortex around the stern bulb, as shown in Fig. 5.

It is worthwhile to note that the KVLCC model shows a clear saddle line at the middle depth, associated with the flow bifurcation into two branches. One converges toward the waterplane and the other converges to the propeller boss (Sotiropoulos & Patel 1995).

Mean velocity distribution

The mean velocity components in the X , Y , Z coordinate are denoted by U , V , W and nondimensionalized by the free-stream velocity U_o . Figures 4 and 5 show the spatial distributions of mean velocities U , V , and W for two ship models at several downstream locations. The main streamwise velocity U/U_o is represented as contour lines, and cross-flow velocity components V and W are represented as velocity vectors. The distances B (breadth), D (draft) are normalized by the length L_{pp} between perpendiculars of the model ship.

The axial mean velocity distributions for the KCS model shown in Fig. 4 do not show any flow reversal in the whole measurement sections. The shear layer formed near the hull surface develops as the flow moves downstream. In the stern region where the cross-sectional area of the hull is decreasing, the shear layer is much thicker than that of the midship region. This mainly results from the rapidly decreasing stern geometry, more than from the history of the upstream flow (Patel 1988).

In the midship region, the cross-flow velocity components V , W are very weak and the boundary layer is thin, compared with the stern region. Near the waterline ($Z/L_{pp} = 0$) of Station 6, the cross-flow is nearly zero and the boundary layer thickness is thinner than that at the turn of the bilge. The thick boundary layer at this turn of the bilge may be attributed to the flow convergence over some distance upstream. At Station 4, a little downstream from Station 6, the boundary layer at the convex hull surface becomes thicker than that at the region of the keel and waterline, indicating flow convergence toward the region of decreasing cross-sectional area. The cross-flow becomes significant from the region of waterline. At the transverse section of Station 2, the cross-flow velocity components are increased and directed toward the concave hull surface, forming a somewhat thick shear layer.

Approaching the stern, the axial velocity U is largely retarded and distorted near the bilge. At Station 1, we can see a steep velocity gradient and vortical structure in the side of the bilge, indicating a formation of vortices. At the propeller plane (Station 0.35), a highly three-dimensional flow is formed in the lower region beneath the propeller boss. The axial velocity decreases remarkably up to $U/U_o = 0.2$ along the vertical centerline. But we cannot find a hook-shaped structure formed for the hull form of VLCC tanker having a large block coefficient (Lee et al 1998). The cross-flow contours show the large-scale bilge vortex. This bilge vortex maintains its shape in the consecutive stations. Other secondary vortices are located near the waterline, but their strength is relatively weak.

At the propeller plane, the mean velocity distributions clearly show the longitudinal vortex located at the depth of $-0.01 \leq Y/L_{pp} \leq -0.005$. In this station, the velocity deficit along the vertical centerline has the largest value among stations tested in this study. As the flow moves downstream in the near-wake region, the

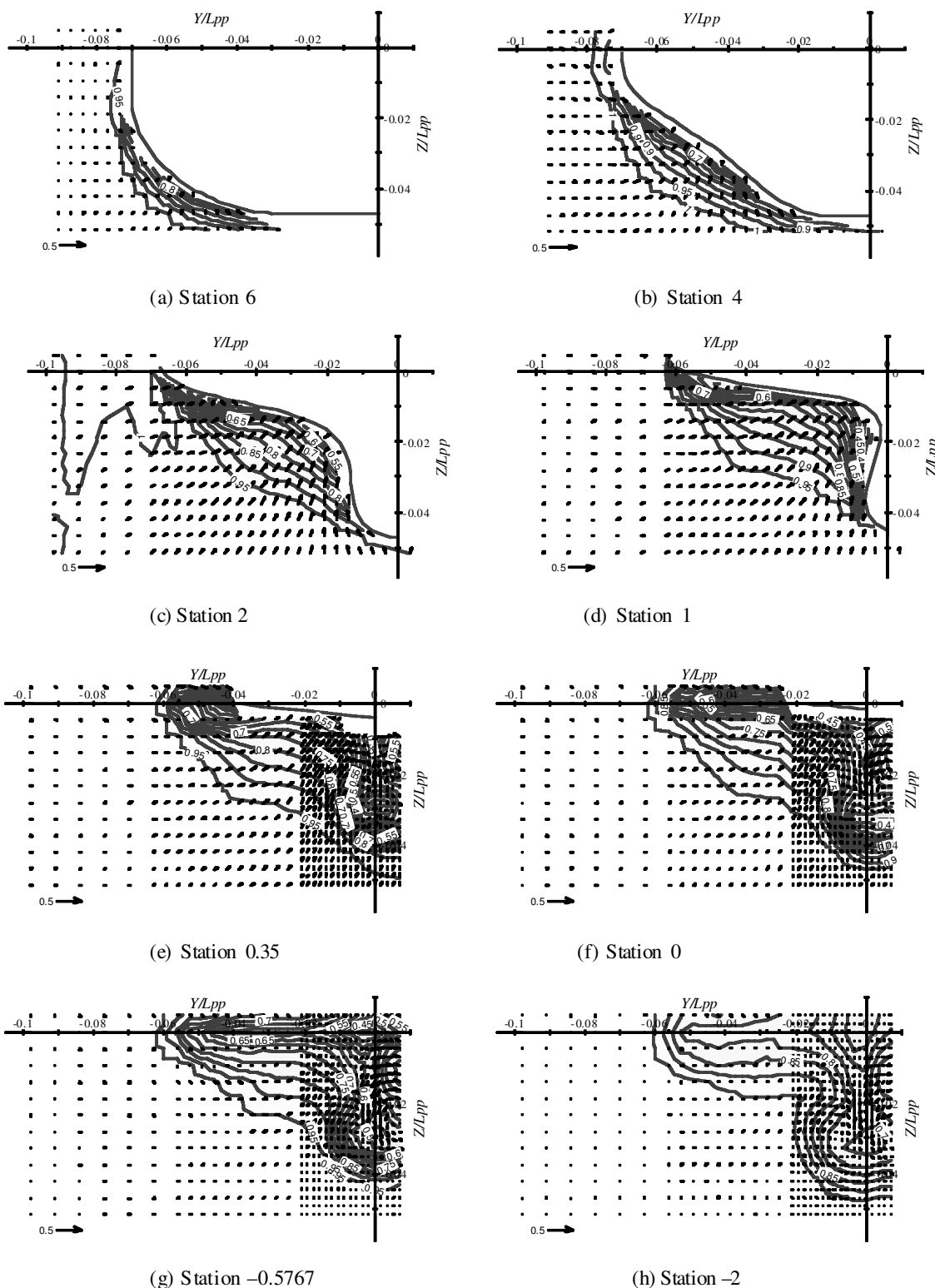


Fig. 4 Axial velocity (U/U_o) contours and transverse ($V/U_o, W/U_o$) vectors for the Korea Research Institute of Ships and Ocean Engineering (KRISO) 3,600 TEU containership (KCS) model

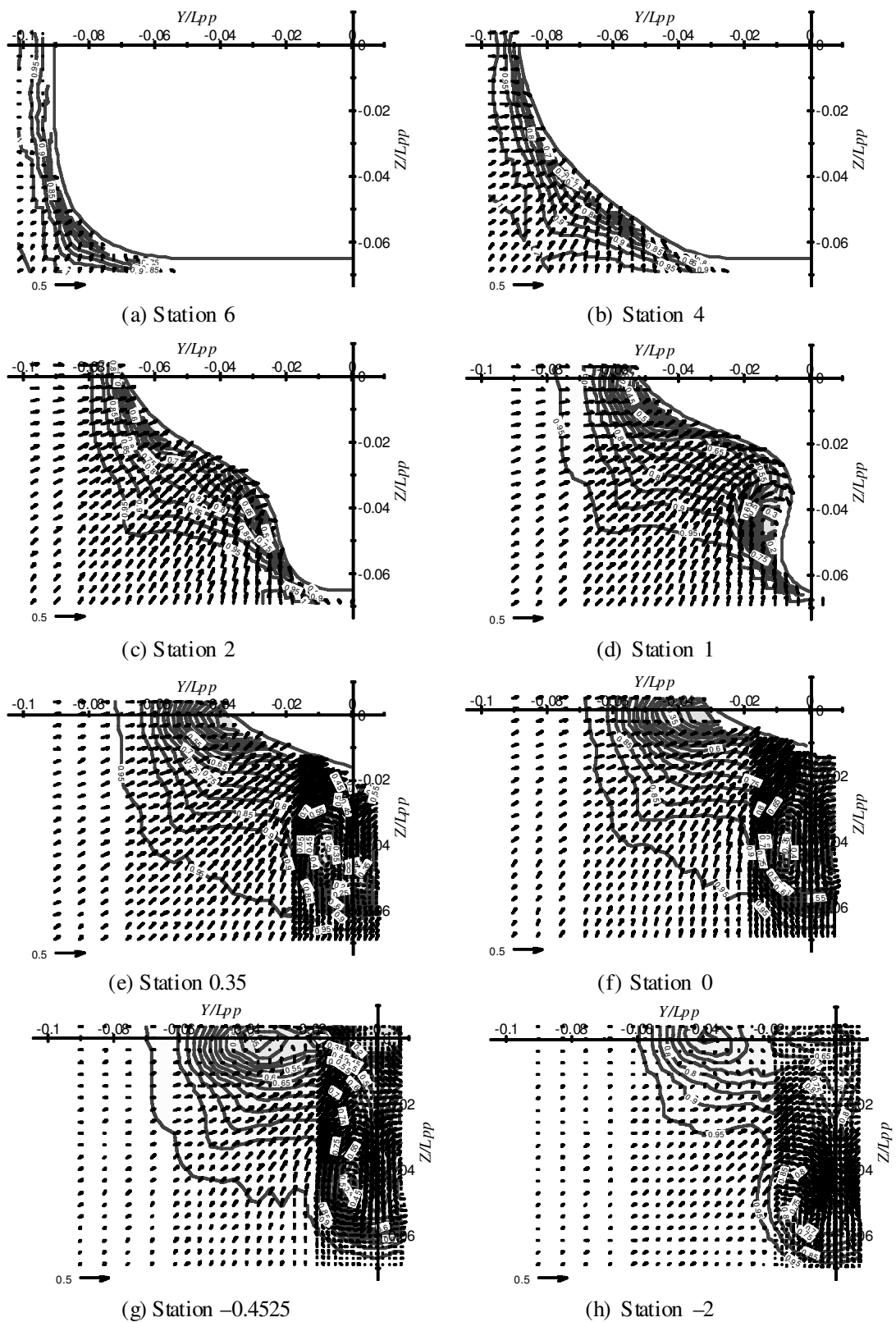


Fig. 5 Axial velocity (U/U_0) contours and transverse velocity ($V/U_0, W/U_0$) vectors of the KRISO 300K VLCC (KVLCC) model

shear layer around the longitudinal vortex expands and its center location is shifted downward. At Station -2, the axial velocity U is recovered up to 70% in the wake centerline and the cross-flow is nearly zero except in the bilge vortex region. Due to strong entrainment of inviscid flow into the near-wake region, the axial velocity contours are somewhat distorted and slowly recover the freestream velocity.

The mean velocity fields for the KVLCC model are shown in Fig. 5. The contours of axial velocity show no region of flow reversal, and the shear layer develops and its thickness increases as the flow moves downstream from the middle ship to the stern. The general flow structures in the middle ship region are similar to those of the KCS model.

Figure 5a shows the normalized mean velocity distributions at Station 6. Near the waterline ($Z/L_{pp} = 0$) and keel, the cross-flow is very weak and the boundary layer thickness is smaller than that at the turn of the bilge. The thick boundary layer is attributed to the flow convergence toward the bilge region over some upstream distance. At Station 4, the boundary layer at the convex hull surface becomes much thicker than that at the region of the keel and waterline, indicating flow convergence toward this region of decreasing cross-sectional area. At Station 2, the cross-flow velocities (V, W) are increased and directed to the concave hull surface, forming a somewhat thick shear layer in this region. Near the waterline of Station 2, the vertical velocity component W is nearly zero due to flow symmetry and the flow is directed beamwise to the hull surface perpendicularly.

At Station 1, in which the hull offset is dramatically changed, the axial velocity U is largely retarded and distorted near the bilge, which may result from the formation of the longitudinal vortex. The cross-flow converges in the hollow stern region and forms a large-scale vortex near the stern bulb. As the cross-sectional area of the KVLCC model abruptly decreases, the boundary layer developed along the hull surface is separated due to a large adverse pressure gradient and forms a thick shear layer. The shear layer near the waterline is much thicker than that near the keel.

At the propeller plane (Station 0.35), the axial velocity contours are strongly distorted and form a longitudinal bilge vortex, as shown in Fig. 5e. Due to the bilge vortex, the entrained cross-flow moves downward along the vertical centerline ($Y = 0$). In the center of the longitudinal vortex, the axial flow is strongly decreased down up to $U/U_o = 0.2$ at the center ($Z/L_{pp} \approx -0.008$) of the longitudinal vortex. The longitudinal bilge vortices of the KVLCC model are vertically elongated and have a much larger velocity deficit, compared with those of the KCS hull form. The bilge vortex maintains its flow structure in the consecutive downstream stations. The measured velocity contours show the so-called hooklike shape in the central part of the wake ($-0.005 \leq Y/L_{pp} \leq 0.018$). This hook-shaped flow pattern was not observed for the KCS model the block coefficient and draft of which are much smaller than the KVLCC model. As the cross-flow approaches the hull surface, the flow moves upward and causes a secondary vortex centered at ($Y/L_{pp} = -0.035, Z/L_{pp} = -0.004$) near the waterline. Its strength is much smaller than that of the longitudinal bilge vortex. The longitudinal vortex at the waterline of the KVLCC model has nearly a circular shape. However, that for the KCS hull form has an elongated shape along the waterline.

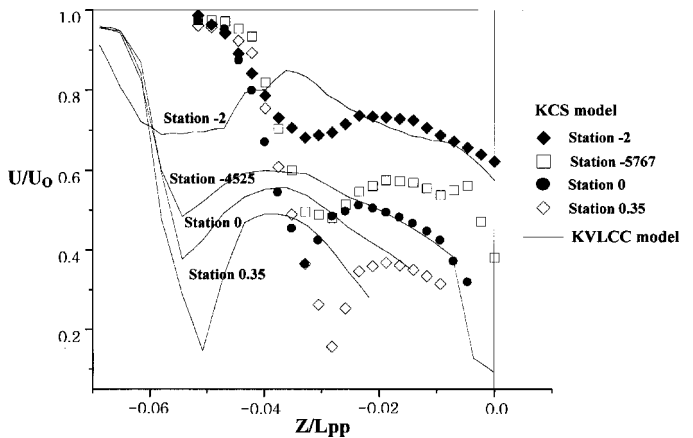


Fig. 6 Comparison of axial mean velocity in the vertical centerline ($Y/L_{pp} = 0$). KCS = Korea Research Institute of Ships and Ocean Engineering (KRISO) 3,600 TEU containership; KVLCC = KRISO 300K VLCC

The mean velocity distributions at Station 0, AP (after perpendicular) of the ship model, also clearly show the large velocity deficit in the wake center region and the longitudinal vortex the center of which is located at $-0.01 \leq Y/L_{pp} \leq 0$. In this station, the velocity deficit is a little recovered, compared with the propeller plane (Station 0.35), and the center of the bilge vortex is lightly shifted downward.

At Stations -0.4525 and -2 in the near-wake region, the flow shows the typical wake structure of bluff bodies. The axial velocity U is recovered up to 70% at Station -2. As the flow moves downstream, the shear layer around the longitudinal vortex expands and its center location is shifted downward due to the entrainment of inviscid flow into the wake region. The axial velocity outside the longitudinal vortex increases, while the cross-flow velocity components V, W are decreased. On the other hand, the secondary vortex located at the midgirth tends to move toward the waterplane as the flow moves from the stern to the wake region. At Station -2, the shear layer near the waterplane shrinks greatly, compared with Station -0.4525. The flow with small momentum is located near the waterline due to the flow convergence along the upper edge of the hollow stern framelines.

The profiles of the axial velocity component along the vertical centerline of symmetry for the KCS and KVLCC hull forms are represented in Fig. 6. The general shape of velocity profiles shows a somewhat similar trend for both models. The location of local minimum velocity is shifted away from the waterline as the flow moves downstream. In addition, the local minimum velocities have nearly the same value at the same stations of both the KCS and KVLCC models. However, the local minimum velocity for the KVLCC model occurs at a much lower depth from the waterline, compared with that of the KCS model at corresponding stations. These seem to be closely related to the evolution of large-scale bilge vortices.

Turbulence statistics

The turbulence statistics, including Reynolds stresses and turbulent kinetic energy, for both models are normalized by U_o^2 in the presentation of the results. Generally, the turbulence quantities in the midship are much smaller than those of the near-wake

region. The Reynolds stresses increase and have the largest values near Station 0 and then decrease as the flow goes downward.

Figures 7 to 9 show the spatial evolution of Reynolds normal stresses \bar{u}^2 , \bar{v}^2 , and \bar{w}^2 for each ship model along the flow direction. The square root of normal stresses normalized by U_o represents the turbulence intensities of each velocity component. Comparing the three normal stresses, the streamwise turbulence intensity \bar{u}^2 is larger than the other two stresses \bar{v}^2 and \bar{w}^2 irrespective of downstream location. This indicates that the flow in the stern and near-wake region has an anisotropic turbulence structure that is typical for most three-dimensional turbulence flows. The anisotropic structure is related to the extra rates of strain, associated with flow convergence and divergence around the stern hull form.

Figure 7 shows the Reynolds normal stress \bar{u}^2 for the KCS and KVLCC models at several stations in the stern and near-wake region. In the case of the KCS model, the streamwise turbulence intensity \bar{u}^2 at Station 2 has small values in the whole measurement locations, even though the corresponding result is not shown in Fig. 7 due to space limitation. At this station, other turbulence quantities \bar{v}^2 and \bar{w}^2 also have small values. All these data are available on the website (<http://www.postech.ac.kr/me/efml/data>).

The streamwise turbulence intensity for the KVLCC model also has very small values at Station 2. However, it is increased relatively greatly at Station 1. The other two normal stresses \bar{v}^2 and \bar{w}^2 also show a similar trend. This may be attributed to the fact that the KVLCC model has a larger block coefficient (C_B) than the KCS model. As the flow goes downstream, the normal stresses \bar{u}^2 , \bar{v}^2 , and \bar{w}^2 increase and have maximum values around Station 0.35 and then decrease slightly with expansion of the shear layer in the near-wake region. At Station 0.35 of the KCS model, the normal stresses have large values at the bottom and side regions of the longitudinal bilge vortex behind the propeller boss. The bottom and lower side regions of the longitudinal vortex have especially large values of Reynolds normal stresses.

In the near-wake region, the streamwise turbulence intensity \bar{u}^2 for the KVLCC model has similar contour lines of the axial mean velocity U shown in Fig. 5. The magnitude of streamwise turbulence intensity in the region of longitudinal bilge vortex behind the propeller boss is larger than that of the KCS model. Other turbulence intensities \bar{v}^2 and \bar{w}^2 of cross-flow velocity components also have larger values in this region where the axial mean velocity has a large velocity gradient, compared with the KCS hull form. It is interesting to note that the region having large values of turbulence intensities for the KVLCC model show the hooklike shape around the longitudinal bilge vortex. As the flow moves downstream, the normal stresses of the KVLCC model are also decreased gradually with expansion of the wake region. However, the decreasing rate is larger than that of the KCS model.

In the case of the KCS hull form, the distributions of \bar{v}^2 and \bar{w}^2 are different from the streamwise normal stress \bar{u}^2 . The axial turbulence intensity is nearly zero along the wake centerline above the center height of the longitudinal vortices; however, the other two turbulence intensities \bar{v}^2 and \bar{w}^2 have relatively large values. In addition, the values of \bar{v}^2 and \bar{w}^2 are smaller than that of \bar{u}^2 in the region of the longitudinal bilge vortex behind the propeller boss in all downstream stations. However, the spatial distributions of the three turbulence intensities for the KVLCC hull form have a nearly similar pattern, although the

cross-flow components \bar{v}^2 and \bar{w}^2 are smaller than the axial turbulence intensity \bar{u}^2 up to Station -0.4525. The difference in the magnitude of the three turbulence intensities is decreased, as the flow moves close to Station -2. This confirms the recovery of the isotropic turbulence structure. However, the KCS hull form does not establish the isotropic turbulence structure at Station -2 due to expansion of the near-wake.

Note that in the middle hollow region, having a thick shear layer in the mean velocity results, the three normal stresses are smaller than those of the surrounding area. This may be attributed to the entrainment of ambient inviscid flow into the hollow stern region. The hook-shaped turbulence structure of the three normal stresses around the longitudinal bilge vortices for the KVLCC hull form is a distinguishing feature, compared with the U shape of the KCS model.

Figures 10 and 11 show the distributions of Reynolds shear stresses $\bar{u}'\bar{v}'$ and $\bar{u}'\bar{w}'$ for both the KCS and the KVLCC models at four downstream stations. Because the mean velocity components V and W are much smaller than the axial velocity U , their gradient in the X -direction, i.e., $\partial V/\partial X$, $\partial W/\partial X$, can be nearly neglected, and the fluctuating velocity components v' and w' are smaller than the streamwise velocity component u' . Therefore, Reynolds shear stresses $\bar{u}'\bar{v}'$ and $\bar{u}'\bar{w}'$ related to the large strain rate $\partial U/\partial Y$, $\partial U/\partial Z$ are more significant than the other shear stress $\bar{v}'\bar{w}'$. Due to flow symmetry, Reynolds shear stress $\bar{u}'\bar{w}'$ is zero on the waterplane ($Z/L_{pp} = 0$), while shear stress $\bar{u}'\bar{v}'$ is zero on the vertical centerline ($Y/L_{pp} = 0$). Therefore, Reynolds shear stresses $\bar{u}'\bar{v}'$ and $\bar{u}'\bar{w}'$ have different distributions.

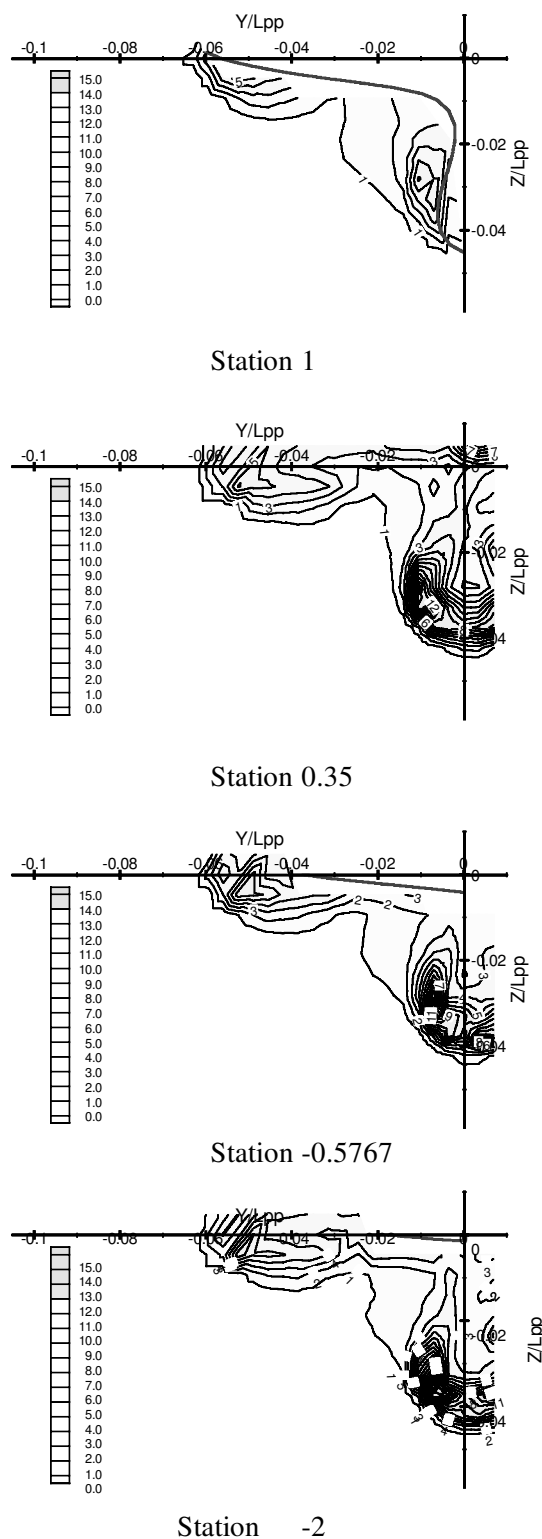
From Figs. 10 and 11, we can see the effect of the longitudinal vortex behind the propeller boss on Reynolds shear stresses $\bar{u}'\bar{v}'$ and $\bar{u}'\bar{w}'$. For the KCS model, Reynolds shear stress $\bar{u}'\bar{v}'$ has the maximum value in the center of the longitudinal bilge vortex and its location is convected downward without much change in the overall distributions shape down to Station -0.5767. Close to Station -2, however, the shear stress is decreased and the shear layer slowly expands due to viscous dissipation. Reynolds shear stress $\bar{u}'\bar{w}'$ shows somewhat flat contours parallel to the waterline in the region behind the propeller boss, which is quite different from the $\bar{u}'\bar{v}'$ distributions.

For the KVLCC model, Reynolds shear stress $\bar{u}'\bar{v}'$ shows vertically elongated contours parallel to the wake centerline, while shear stress $\bar{u}'\bar{w}'$ has the hook-shape contours in the near-wake behind the propeller boss. Reynolds shear stresses $\bar{u}'\bar{v}'$ and $\bar{u}'\bar{w}'$ have local maximum values at the lateral location of $Y/L_{pp} = -0.015$ and $Y/L_{pp} = 0$, respectively. The location of maximum shear stress moves gradually downward, as the flow moves downstream.

The contours of turbulent kinetic energy, defined as $k = \rho/2(\bar{u}^2 + \bar{v}^2 + \bar{w}^2)/U_o^2$, for both the KCS and the KVLCC models are shown in Fig. 12. The contours of turbulent kinetic energy are similar to those of streamwise turbulence intensity \bar{u}^2 . This results from the fact that the streamwise normal stress \bar{u}^2 is much larger than the other two normal stresses \bar{v}^2 and \bar{w}^2 . Therefore, the turbulent kinetic energy has large values in the high shear region having large velocity gradient of axial velocity component.

On average, the turbulent kinetic energy in the near-wake region of the KCS model is smaller than half of the turbulent kinetic energy in the near-wake region of the KVLCC hull form. In the near-wake region, the kinetic energy has maximum value

(a) KCS model



(b) KVLCC model

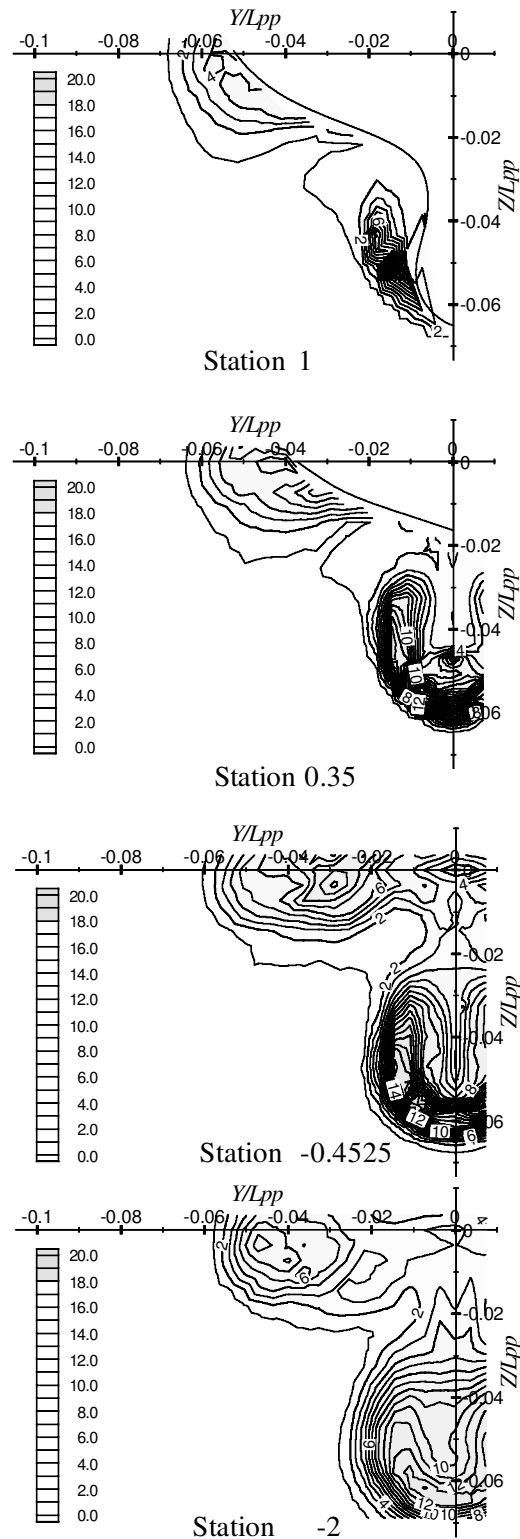
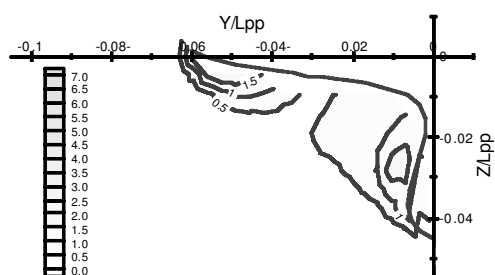
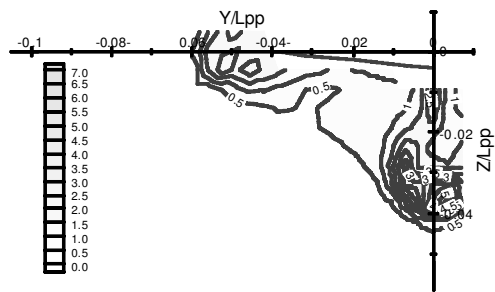


Fig. 7 Distributions of Reynolds normal stress \bar{u}^2/U_o^2 ($\times 10^3$) for the Korea Research Institute of Ships and Ocean Engineering (KRISO) 3,600 TEU containership (KCS) and KRISO 300K VLCC (KVLCC) models

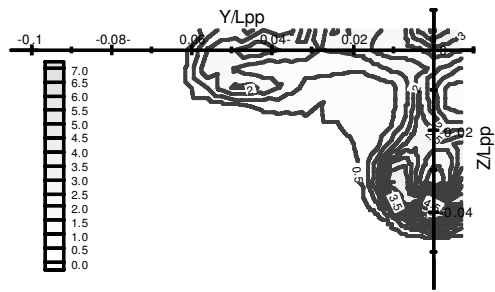
(a) KCS model



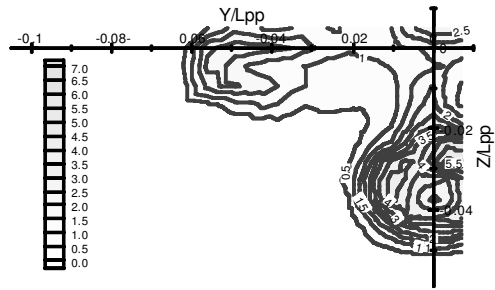
Station 1



Station 0.35

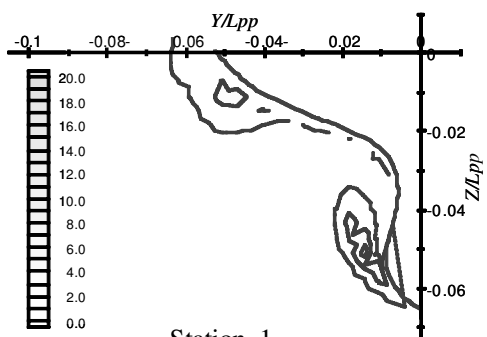


Station -0.5767

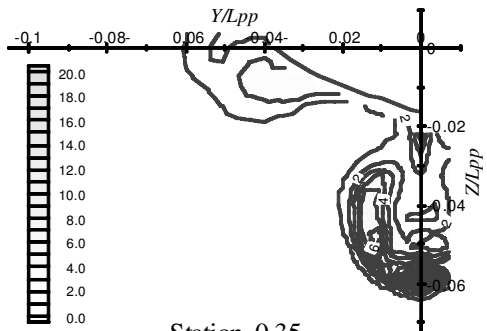


Station -0.2

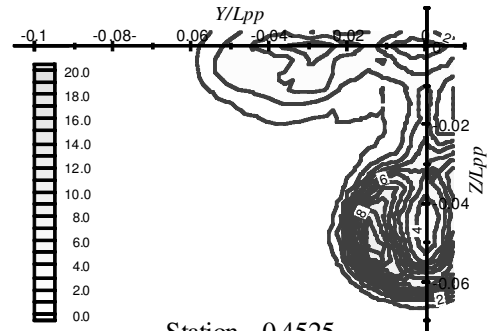
(b) KVLCC model



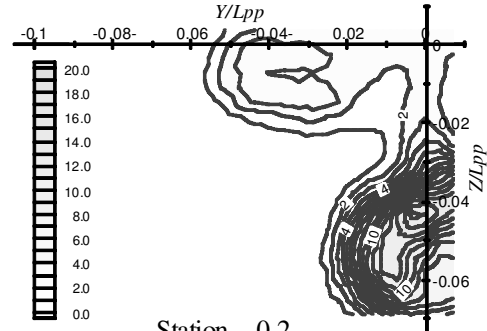
Station 1



Station 0.35



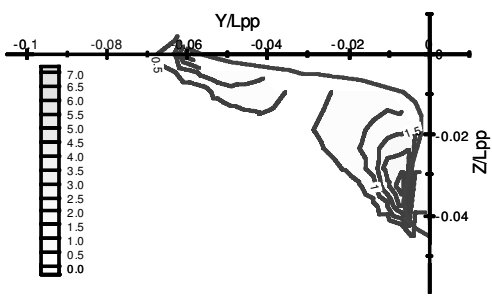
Station -0.4525



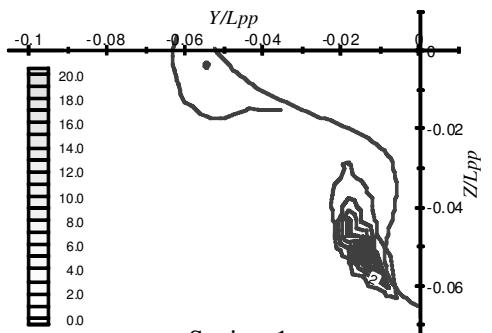
Station -0.2

Fig. 8 Distributions of Reynolds normal stress $\bar{v}^2/U_o^2 \times 10^3$ for the Korea Research Institute of Ships and Ocean Engineering (KRISO) 3,600 TEU containership (KCS) and KRISO 300K VLCC (KVLCC) models

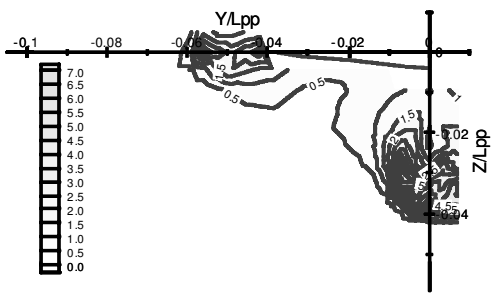
(a) KCS model



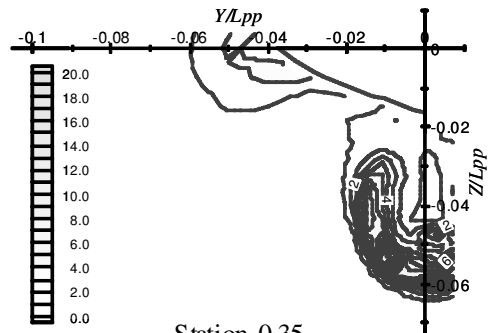
(b) KVLCC model



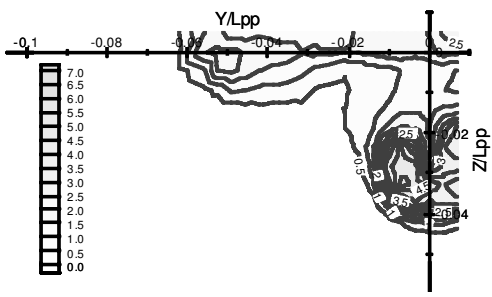
Station 1



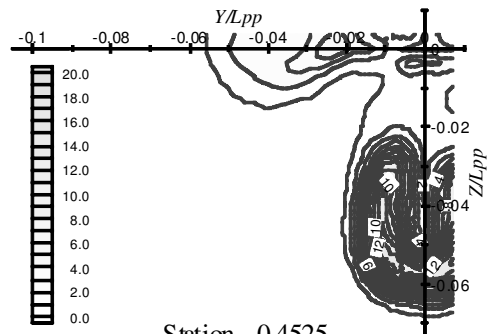
Station 1



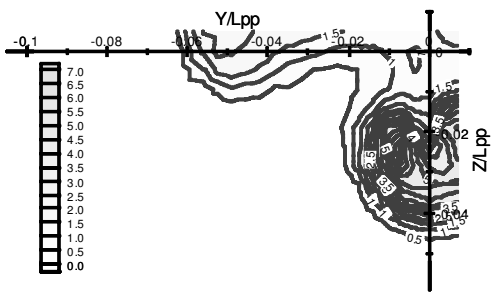
Station 0.35



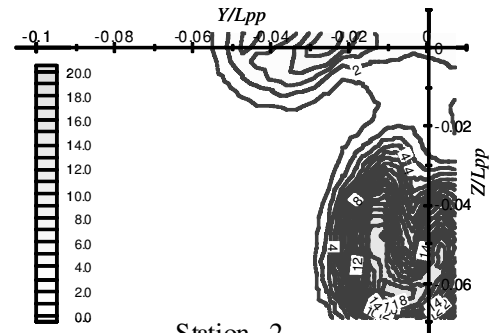
Station 0.35



Station -0.5767



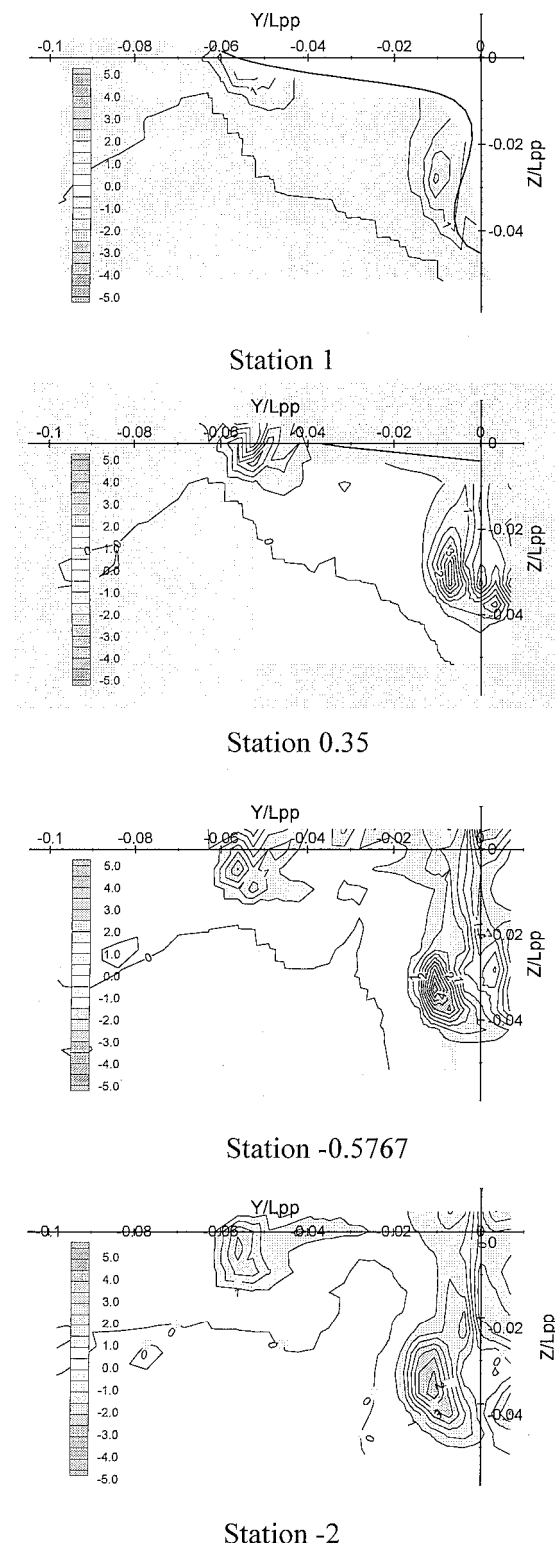
Station -0.5767



Station -2

Fig. 9 Distributions of Reynolds normal stress $\bar{w}^2/U_o^2 (\times 10^3)$ for the Korea Research Institute of Ships and Ocean Engineering (KRISO) 3,600 TEU containership (KCS) and KRISO 300K VLCC (KVLCC) models

(a) KCS model



(b) KVLCC model

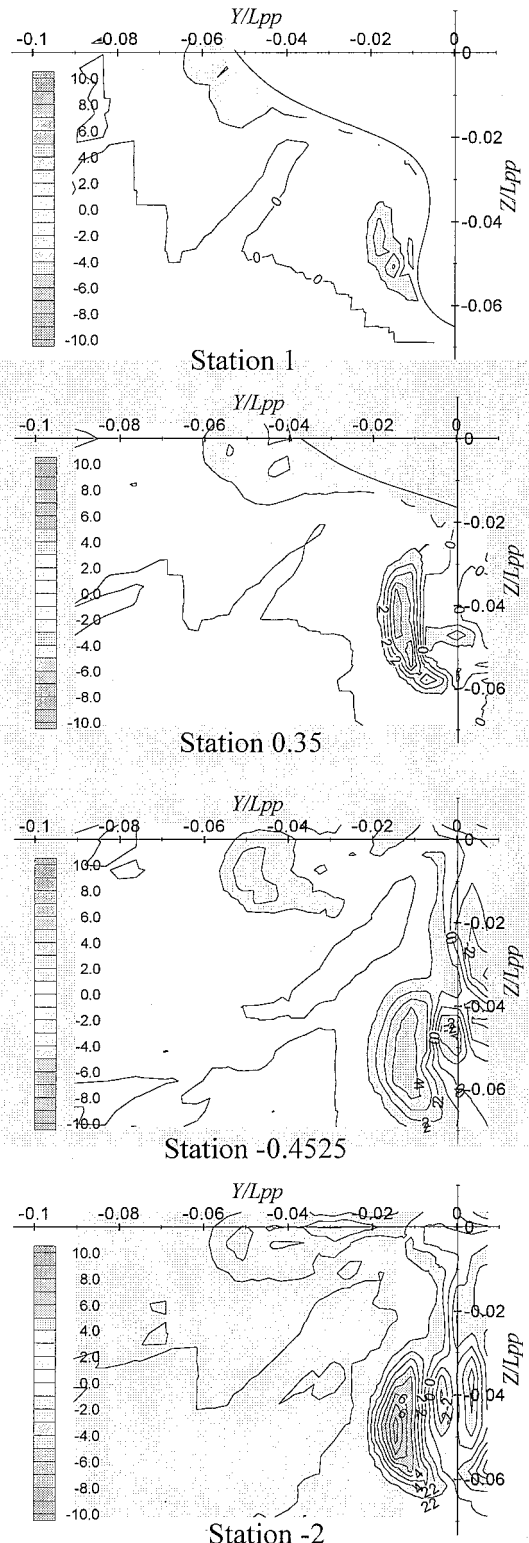
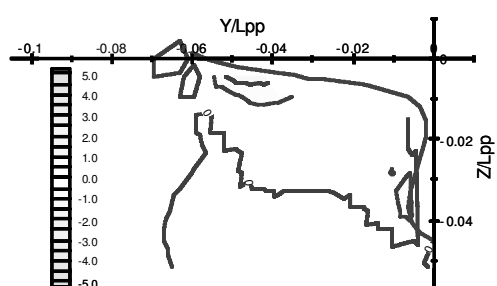
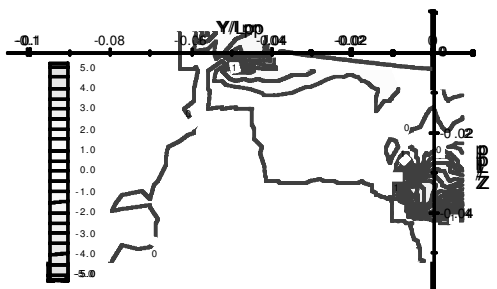


Fig. 10 Distributions of Reynolds shear stress $\bar{u}\bar{v}'/U_o^2$ ($\times 10^3$) for the Korea Research Institute of Ships and Ocean Engineering (KRISO) 3,600 TEU containership (KCS) and KRISO 300K VLCC (KVLCC) models

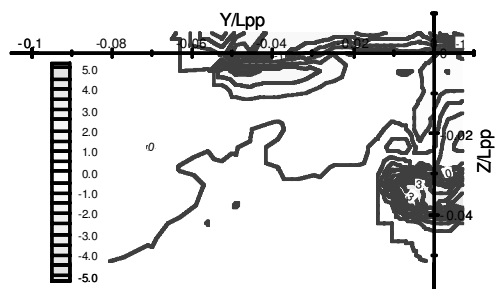
(a) KCS model



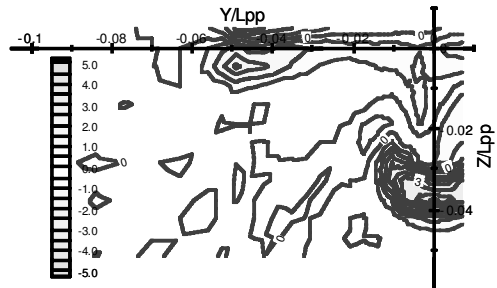
Station 1



Station 0.35

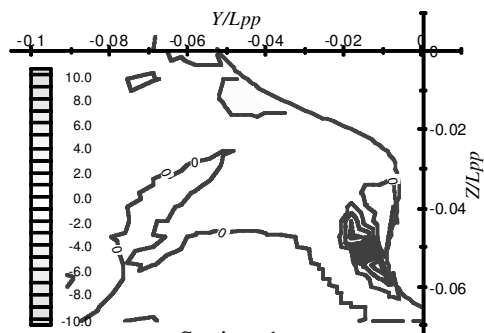


Station -0.5767

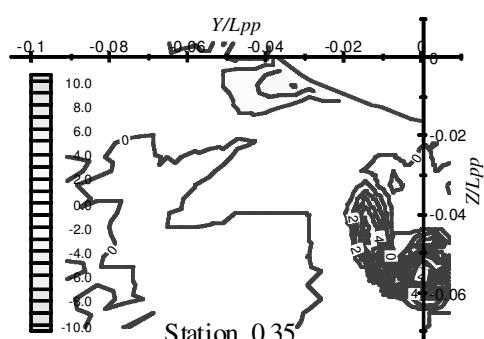


Station -2

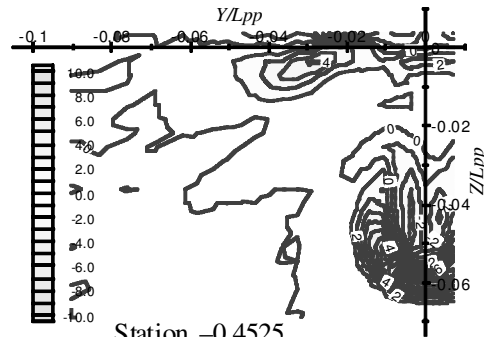
(b) KVLCC model



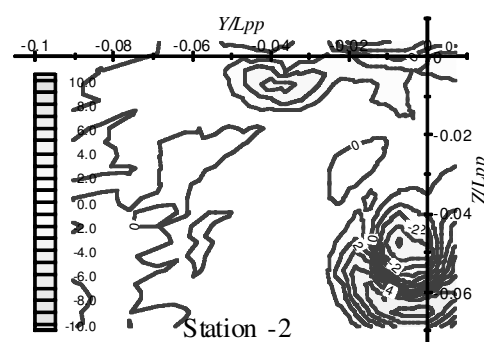
Station 1



Station 0.35



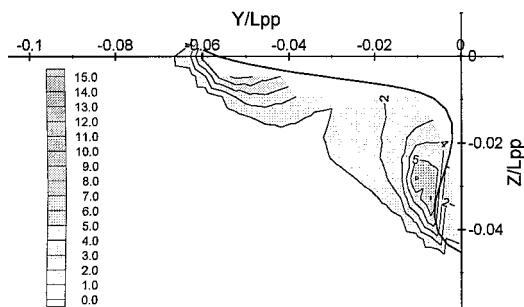
Station -0.4525



Station -2

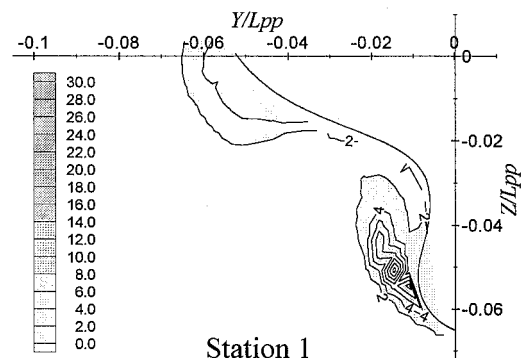
Fig. 11 Distributions of Reynolds shear stress $\overline{u'w'}/U_o^2$ ($\times 10^3$) for the Korea Research Institute of Ships and Ocean Engineering (KRISO) 3,600 TEU containership (KCS) and KRISO 300K VLCC (KVLCC) models

(a) KCS model

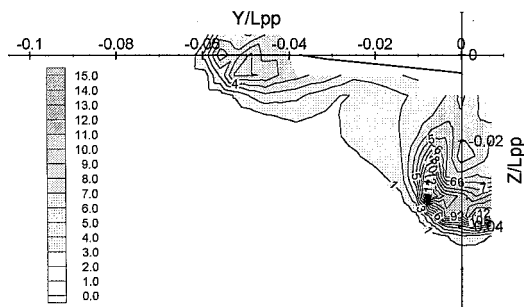


Station 1

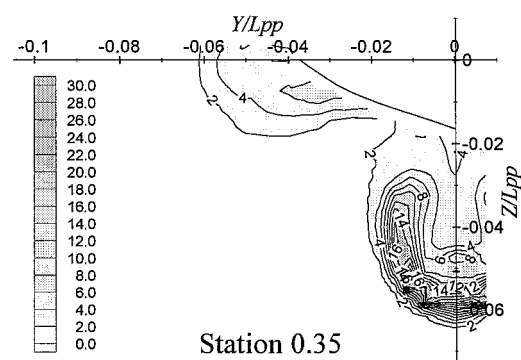
(b) KVLCC model



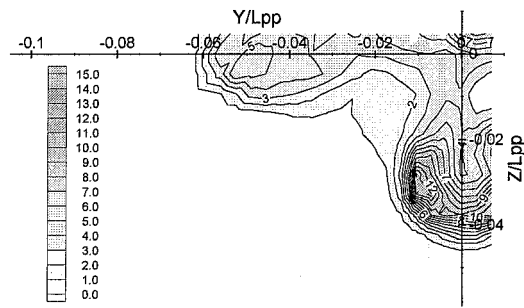
Station 1



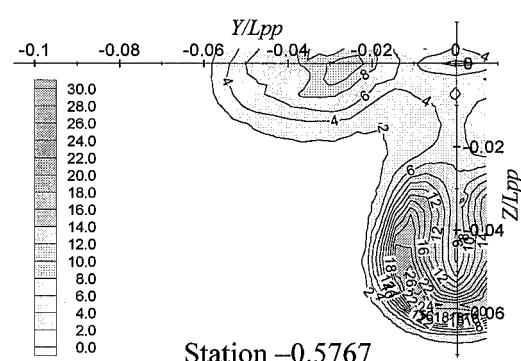
Station 0.35



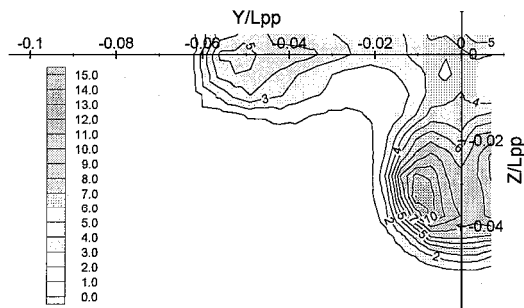
Station 0.35



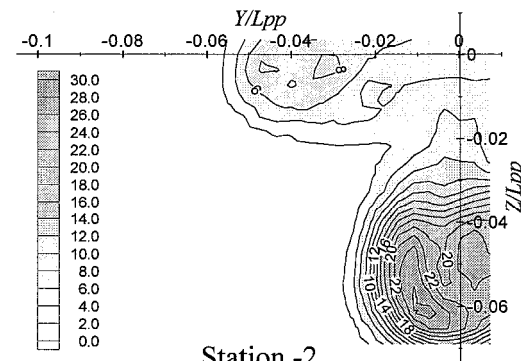
Station -0.5767



Station -0.5767



Station -2



Station -2

Fig. 12 Distributions of turbulent kinetic energy $k = \frac{\rho}{2}(\bar{u}^2 + \bar{v}^2 + \bar{w}^2)/U_o^2 (\times 10^3)$ for the Korea Research Institute of Ships and Ocean Engineering (KRISO) 3,600 TEU containership (KCS) and KRISO 300K VLCC (KVLCC) models

at a depth of about $Z/L_{pp} = -0.036$, whereas the KVLCC model has maximum kinetic energy at $Z/L_{pp} = -0.058$. This may be closely related to the vertical location of the maximum velocity deficit of streamwise mean velocity for both ship models. These results indicate that the KCS hull form was designed to have small turbulence statistics in the stern and near-wake regions, from the hydrodynamics point of view. As can be expected from the mean velocity results, for the KCS model, the size of the shear layer in which the turbulence statistics have significant values is smaller than that of the KVLCC hull form.

The wind tunnel experimental data for a double-deck ship model was assumed to be the same as the towing tank data. The comparison of these data under the same experimental condition is required as a future study.

Concluding remarks

The flow characteristics around the KCS and KVLCC double-deck ship models have been experimentally investigated in a subsonic wind tunnel. The local mean velocity and turbulence statistics in the stern and near-wake regions were measured using an x -type hot-wire probe.

The mean velocity distributions show clearly the flow characteristics in the stern and near-wake region. For both ship models, the shear layer at the midship develops over the stern and evolves into a complicated three-dimensional wake. The shear layer at the concave stern region is thick due to the entrainment of inviscid fluid into the region. Two longitudinal vortices are formed in the stern region due to convergence of cross-flow: one around the propeller boss and the other near the waterline. The longitudinal vortices influence dominantly the flow structure in the near-wake region. In the region of the large-scale longitudinal bilge vortex, the turbulence statistics have higher values, compared with the surrounding regions. For the KCS model, the shear layer in the stern and near-wake regions is smaller than that of the KVLCC hull form.

The longitudinal vortex at the waterline of the KVLCC model has a nearly circular shape; however, that for the KCS hull form has an elongated shape along the waterline. The longitudinal bilge vortices of the KVLCC model have a much larger velocity deficit and vertically elongated shape, compared with those of the KCS hull form. The KVLCC model has large values of turbulence intensity and turbulent kinetic energy in the hook-shaped regions around the longitudinal bilge vortex. On the contrary, the KCS model also has large values of turbulence statistics in a U-shaped region around the bilge vortex. The turbulence statistics for the KVLCC model are much larger than those of the KCS model.

In the near-wake regions of both ship models, the streamwise normal stress \bar{u}^2 is larger than the other two normal stresses \bar{v}^2 and \bar{w}^2 , indicating the anisotropic turbulence structure. As the flow moves downstream, the values of turbulence statistics are increased, have maximum value at Station 0.35, and then decrease gradually. The decreasing rate of streamwise turbulence intensity \bar{u}^2 for the KVLCC model is larger than that of the KCS model. The near-wake region nearly recovers the isotropic turbulence

structure at Station -2. However, the KCS model still holds the anisotropic structure at Station -2 due to slow expansion of the near-wake region.

The complete experimental data set is available on the website (<http://www.postech.ac.kr/me/efml/data>). These data can be used comparatively to validate the numerical simulations and turbulence models for modern hull forms.

Acknowledgments

This research was financially supported by the Korea Research Institute of Ships and Ocean Engineering (KRISO). The authors appreciate the support of Professor C. M. Lee, Mr. M. S. Koh, and Mr. B. G. Paik of Pohang University of Science and Technology.

References

- Gietz, U. and Ku, J. 1995 Flow investigations on the Hamburg test case model in the wind tunnel. Institut Für Schiffbau Der Universität Hamburg, Bericht Nr. 550.
- Hockstra, M. and Aallers, A. 1997 Macro wake measurements for a range of ships. *Proceedings, 21st Symposium on Naval Hydrodynamics*, Washington, D.C., 278–290.
- Hoffman, H. P. 1976 Untersuchung der 3-dimensionalen, turbulenten grenzschicht an einem Schiffsmodell in windkanal. Institut Für Schiffbau Der Universität Hamburg, FRG, Report No. 343.
- ITTC 1987 Report of the resistance and flow committee, *Proceedings, 18th International Towing Tank Conference*, 1, Kobe, Japan, 47–95.
- ITTC 1999 Quality manual. S. I. Yang, Ed., *Proceedings, 22nd International Towing Tank Conference (ITTC)*, Seoul, Korea/Shanghai, PR China.
- Kim, W. J., Van, S. H., and Kim, D. H. 2001 Measurement of flows around modern commercial ship models. *Experiments in Fluids*, **31**, 567–578.
- Knaack, T., Kux, J., and Wieghardt, K. 1985 On the structure of the flow field on ship hulls. *Proceedings, Osaka International Colloquium on Ship Viscous Flow*, Osaka, Japan, 192–208.
- Larsson, L. 1974 Boundary layers of ships, part III: An experimental investigation of the turbulent boundary layer on a ship model. *SSPA*, Gothenburg, Sweden, Report No. 46.
- Larsson, L., Stern, F., and Bertram, V. 2000 Gothenburg 2000: A workshop on numerical ship hydrodynamics, Gothenburg, Sweden.
- Lee, J. H., Lee, S. J., and Van, S. H. 1998 Wind tunnel test on a double deck shaped ship model. *Proceedings, 3rd International Conference on Hydrodynamics*, 2, Seoul, Korea, 815–820.
- Löfdahl, L. 1982 Measurement of the Reynolds stress tensor in the thick three-dimensional boundary layer near the stern of a model ship. *SSPA*, Gothenburg, Sweden, Report No. 61.
- Patel, V. C. 1988 Ship stern and wake flows: Status of experiment and theory. Iowa Institute of Hydraulic Research, University of Iowa, IIHR Report No. 323.
- Patel, V. C. and Sarda, O. P. 1990 Mean-flow and turbulence measurements in the boundary layer and wake of a ship double model. *Experiments in Fluids*, **8**, 319–335.
- Sotiroupolos, F. and Patel, V. C. 1995 Application of Reynolds-stress transport models to stern and wake flows. *Journal of Ship Research*, **39**, 263–283.
- Toda, Y., Stern, F., Tanaka, I. and Patel, V. C. 1990 Mean-flow measurements in the boundary layer and wake of a series 60 $C_b = 0.60$ model ship with and without propeller. *Journal of Ship Research*, **34**, 225–252.